Supporting Information

NiOOH-Mediated Electron Injection into $Ti_3C_2F_x$ to Weaken Ti-H Bond for Accelerated Photocatalytic Hydrogen Production

Jianming Duanmu[a], Ping Wang[a,b,*], Xuefei Wang[b], Feng Chen[b]

[a]School of Materials Science and Engineering, Wuhan University of Technology, Wuhan 430070, People's Republic of China

[b]School of Chemistry, Chemical Engineering and Life Sciences, Wuhan University of Technology, Wuhan 430070, People's Republic of China

*Corresponding authors. Tel: +86(27)87749379;

E-mail: wangping0904@whut.edu.cn (Ping Wang)

Number of pages: 17

Number of Figures: 8

SI-1 Materials

Ti_3AlC_2 powders (> 98 wt% purity) were purchased from beike 2D materials Co., Ltd, ammonium fluoride (NH_4F), hydrochloric acid (HCl, 38%), dimethyl sulfoxide (DMSO), Nickel(II) chloride hexahydrate ($NiCl_2 \cdot 6H_2O$), Urea, Cadmium acetate dihydrate($CH_3COOCd \cdot 2H_2O$), Sodium Sulfide Decahydrate($Na_2S \cdot 9H_2O$), Sodium sulfite(Na_2SO_3), sodium sulphide (Na_2SO_4) and ethyl-alcohol (C_2H_5OH) were of analytical grade from Shanghai Chemical Reagent Ltd. and used without further purification.

SI-2 Characterization

Microstructures and morphologies of the as-prepared samples were conducted by X-ray diffraction (XRD) ((D/MAXRB, RIGAKU, Japan), Field emission scanning electron microscope (FESEM, JSM 7500F, Japan) and transmission electron microscopy (HRTEM, JEM 2100F, Japan). Elemental analyses of photocatalysts were measured via X-ray photoelectron spectroscopy (XPS) ((ESCALAB 250Xi, Thermo Fisher Scientific, USA). All binding energies in the XPS spectra were calibrated using the peak position of C 1s (284.8 eV). Optical properties were evaluated by UV-Vis spectrophotometry (UV-2450, Shimadzu, Japan) using $BaSO_4$ as reference standard, systematically recording light absorption characteristics across 200-800 nm wavelength range. Photoluminescence dynamics were investigated using an FLS920 fluorescence spectrophotometer (Edinburgh Instruments, UK) equipped with time-correlated single photon counting (TCSPC) system, enabling precise acquisition of

time-resolved photoluminescence (TRPL) spectral data.

SI-3 Photoelectrochemical measurements

Photoelectrochemical (PEC) curves were measured on an electrochemical analyzer (CHI660E, China) in a standard three-electrode configuration according to our previous works[1,2]. The prepared samples were loaded on fluorine-doped tin oxide (FTO) conductor glass, a standard Ag/AgCl electrode and the platinum foil as the working electrodes, reference electrode and counter electrode, respectively, with Na_2SO_4 (0.5 mol L^{-1}) as the electrolyte solution. The method of working electrodes was the same as in our previous works. Linear sweep voltammetry (LSV) curves were obtained in the potential ranging of -1.0 to -1.6 V with a scan rate of 10 mV s^{-1}. Transient photocurrent responses with time (*i-t* curves) were recorded at 0.5 V bias potential during periodic ON/OFF illumination cycles under a 3W LED lamp (365 nm). Electrochemical impedance spectroscopy (EIS) curves were conducted at the frequency range of 0.01-10^5 Hz with an ac amplitude of 10 mV under the open-circuit voltage.

SI-4 Photocatalytic H_2-evolution measurement

The photocatalytic hydrogen evolution performance was evaluated in a standard three-neck quartz photoreactor (250 mL capacity). The reaction system contained 80 mL of an aqueous mixed solution of sodium sulfide and sodium sulfite (specifically, 2.52 g Na_2SO_3 and 6.72 g $Na_2S{\cdot}6H_2O$ dissolved in deionized water) as the sacrificial agent medium. Prior to experiments, the reaction system was purged with high-purity

nitrogen for 30 minutes to establish an inert atmosphere and remove dissolved oxygen. The photoexcitation system consisted of four high-power LED units (central wavelength 365±5 nm, 3 W per lamp) arranged in a circular array, achieving uniform irradiation through optical fibers (light power density approximately 80 mW cm^{-2}). Hydrogen evolution kinetics were monitored via manual sampling. After reaching steady-state hydrogen production rate, 400 μL gas samples were collected hourly using a gas-tight syringe and quantitatively analyzed by a Shimadzu GC-2014C gas chromatograph equipped with a TCD detector and 5 Å molecular sieve column (high-purity argon carrier gas, column temperature 80°C). For cycling stability tests, sampling was performed every 30 minutes. Each cycle was conducted for 120 minutes, followed by opening the gas inlet/outlet valves to inject high-purity nitrogen for 15 minutes before sealing the system for subsequent hydrogen production cycles. The apparent quantum efficiency (AQE) was calculated according to **Equation S1**:

$$\begin{aligned} \mathrm{AQE}(\%) &= \frac{\text{number of reacted eletrons}}{\text{number of incident photons}} \times 100\% \\ &= \frac{\text{mumber of evolved } H_2 \text{ molecules} \times 2}{\text{mumber of incident photons}} \times 100\% \\ &= \frac{2R_{H_2} t_1 N_A}{\frac{EAt_2\lambda}{hc}} \\ &= 6.6482 \times 10^{-5} \times \frac{R_{H_2}}{EA\lambda} \#(S1) \end{aligned}$$

R_{H_2} (μmol h^{-1}) represents the H_2-evolution rate, E (W cm^{-2}) represents the monochromatic light intensity, A (cm^2) represents the light radiation area of the reaction system, λ (m) represents the monochromatic wavelength, while t_1 (h), t_2 (s), h

(W), and c (m s^{-1}) are constants with values of 1, 3600, 6.626×10^{-34} and 3×10^{8}, respectively. In this work, 50 mg of the photocatalyst was irradiated by four 365 nm LED lights as the light source. The light radiation area (A) and the light intensity (E) of the reaction system are 1×4 cm^2 and 80 mW cm^{-2}, respectively.

SI-5 DFT calculations

The calculations were carried out by using the Vienna *ab* initio simulation package (VASP)[3,4]. The generalized gradient approximation (GGA) with Purdew-Burke-Ernzerhof (PBE) functional[5,6] was selected to reveal the exchange-correlation interaction. The cutoff energy and Monkhorst-Pack k-point mesh was set as 450 eV and $3 \times 3 \times 1$, respectively. The convergence threshold d for total energy converged within 10^{-5} eV/atom and 0.01 eV·$Å^{-1}$ for force. To eliminate interactions between periodic structures, a vacuum of 15 Å was added. The Gibbs free energy of H atom adsorption (ΔG_{H*}) was defined as following the equation S2:

$$\Delta G_{H*} = \Delta E_{H*} + \Delta E_{ZPE} - T\Delta S_H \#\#(S2)\#\#\#$$

Where ΔE_{H*}, ΔE_{ZPE}, $T\Delta S_H$ are the differential hydrogen ΔE_{H*} adsorption energy, the change in zero-point energy and entropy between the adsorbed hydrogen and molecular hydrogen in gas phase, respectively, and T is the temperature. The term $T\Delta S_H$ was calculated to be -0.20 eV. Additionally, ΔE_{H*} represents the change in H adsorption energy, which can be defined by the following **Equation S3**:

$$\Delta E_{H*} = \Delta E_{(Surface+H*)} - \Delta E_{(Surface)} - \frac{1}{2}\Delta E_H \#(S3)$$

Where $\Delta E_{(Surface)}$ and $\Delta E_{(Surface+H^*)}$ respectively represent the surface energy of the material and the surface energy of the material with an adsorbed hydrogen atom, while ΔE_H represents the energy of a hydrogen molecule in the gas phase.

In this work, Ti_3C_2 model was constructed by removing Al atom in the Ti_3AlC_2 (002) model. The (3 × 3 × 1) supercell containing 27 Ti and 18 C atoms of crystalline. $Ti_3C_2F_x$ structure was added 18 F atoms on the basis of Ti_3C_2 model and performed for the following theoretical calculations. $Ti_3C_2F_x$ (002) model was composed of 27 Ti atoms, 18 C atoms and 18 F atoms. The NiOOH model was constructed by cleaving along the (002) plane and expanding the primitive cell into a 3×3×1 supercell, comprising 9 Ni atoms, 18 O atoms, and 9 H atoms (36 atoms in total). The work function is defined as $\Phi = E_v - E_f$, where E_v and E_f are the electrostatic potentials of the vacuum and Fermi levels, respectively.

References

[1] R. Liu, P. Wang, X. Wang, F. Chen, H. Yu, Facilitating Oriented Electron Transfer from Cu to Mo_2C MXene for Weakened Mo─H Bond Toward Enhanced Photocatalytic H_2 Generation, Small 21 (2024). DOI: https://doi.org/10.1002/smll.202408330.

[2] Y. Cao, P. Wang, X. Wang, F. Chen, H. Yu, Charge self-regulation of Ti sites in Ti3C2 MXene via rich unsaturated Ti for boosted photocatalytic hydrogen generation, Journal of Materials Chemistry C 12 (2024) 10152-10160. DOI: https://doi.org/10.1039/d4tc01076k.

[3] G. Kresse, J. Hafner, *Phys. Rev. B* 47 (1993) 558. DOI: https://doi.org/10.1103/PhysRevB.47.558.

[4] P.E. Blöchl, *Phys. Rev. B* 50 (1994) 17953. DOI: https://doi.org/10.1103/PhysRevB.50.17953.

[5] J.P. Perdew, K. Burke, M. Ernzerhof, *Phys. Rev. Lett.* 77 (1996) 3865. DOI: https://doi.org/10.1103/PhysRevLett.77.3865.

[6] G. Kresse, D. Joubert, *Phys. Rev. B* 59 (1999) 1758. DOI: https://doi.org/10.1103/PhysRevB.59.1758.

Figure captions

Fig. S1. Photocatalytic H_2-evolution rate of (a) CdS, (b) NiOOH-$Ti_3C_2F_x$(1:5)/CdS-1%, (c) NiOOH-$Ti_3C_2F_x$(1:5)/CdS-5%, and (d) NiOOH-$Ti_3C_2F_x$(1:5)/CdS-10%.

Fig. S2. Photocatalytic H_2-evolution rate of (a) $Ti_3C_2F_x$, (b) NiOOH-$Ti_3C_2F_x$, (c) CdS, (d) $Ti_3C_2F_x$/CdS, and (e) NiOOH-$Ti_3C_2F_x$/CdS.

Fig. S3. Photocatalytic H_2-evolution rate of (a) TiO_2, (b) $Ti_3C_2F_x$/TiO_2, (c) NiOOH-$Ti_3C_2F_x$(1:10)/TiO_2, (d) NiOOH-$Ti_3C_2F_x$(1:5)/TiO_2, and (e) NiOOH-$Ti_3C_2F_x$(1:2)/TiO_2.

Fig. S4. (A) XPS survey spectra and (B) high-resolution spectra of F 1s for (a) $Ti_3C_2F_x$ and (b) NiOOH-$Ti_3C_2F_x$(1:1).

Fig. S5. Front and top views of the optimized models of (A) Ti_3C_2 MXene, (B) $Ti_3C_2F_x$, (C) NiOOH-$Ti_3C_2F_x$.

Fig. S6. The optimized models for DFT calculations of (A) NiOOH; (B) H-NiOOH.

Fig. S7. (A). Top view of the different hydrogen adsorption sites on NiOOH-$Ti_3C_2F_x$; Demonstration of different adsorption sites on NiOOH-$Ti_3C_2F_x$, exemplified by (B). top site of Ti; (C). top site of Ni; (D). top site of C; (E). top site of O.

Fig. S8. (A) Electrochemical impedance spectra (EIS) and (B) linear sweep voltammetry (LSV) curves of (a) CdS, (b) $Ti_3C_2F_x$/CdS, (c) NiOOH-$Ti_3C_2F_x$(1:1)/CdS, and (d) NiOOH-$Ti_3C_2F_x$(1:5)/CdS.

Table S1. The energy dispersive X - ray Spectroscopy (EDS) spectrum obtained by TEM for NiOOH-$Ti_3C_2F_x$(1:1)/CdS.

Element	Counts Mass (%)	Sigma Atom (%)	Compound Mass (%)
Cd	65.15	0.33	26.16
S	17.27	0.12	24.30
Ti	1.27	0.04	1.19
C	9.29	0.08	34.90
Ni	3.11	0.07	2.40
O	3.29	0.06	11.05

Table S2. Fluorescence emission lifetime and relevant percentage data fitted by a three-exponential function.

Samples	τ_1 (ns)	A_1	τ_2 (ns)	A_2	τ_3 (ns)	A_3	Average lifetime(τ_a) (ns)
CdS	0.61	8787.08	3.12	2654.1	12.05	310.47	4.268010242
$Ti_3C_2F_x$/CdS	0.8	9076.31	3.26	2809.5	10.64	372.86	3.819960573
NiOOH-$Ti_3C_2F_x$(1:1)	0.67	9882.08	3.17	2514.6	11.2	297.66	3.740000403
NiOOH-$Ti_3C_2F_x$(1:5)	0.58	9313.96	2.86	2441.5	11.13	262.38	3.633198231

The above-fitted parameters are acquired via the following tri-exponential formulas:

$$I_t = I_0 + A_1\exp(-t/\tau_1) + A_2\exp(-t/\tau_2) + A_3\exp(-t/\tau_3) \quad (5)$$

$$\tau_a = \left(A_1\tau_1^2 + A_2\tau_2^2 + A_3\tau_3^2\right)/\left(A_1\tau_1 + A_2\tau_2 + A_3\tau_3\right) \quad (6)$$

where I_0 is the baseline correction value, A_1, A_2, and A_3 represent the tri-exponential factors, and τ_1, τ_2, τ_3, and τ_a correspond to the lifetime in various stages (radiation, non-radiation, and energy transfer) and average lifetime.

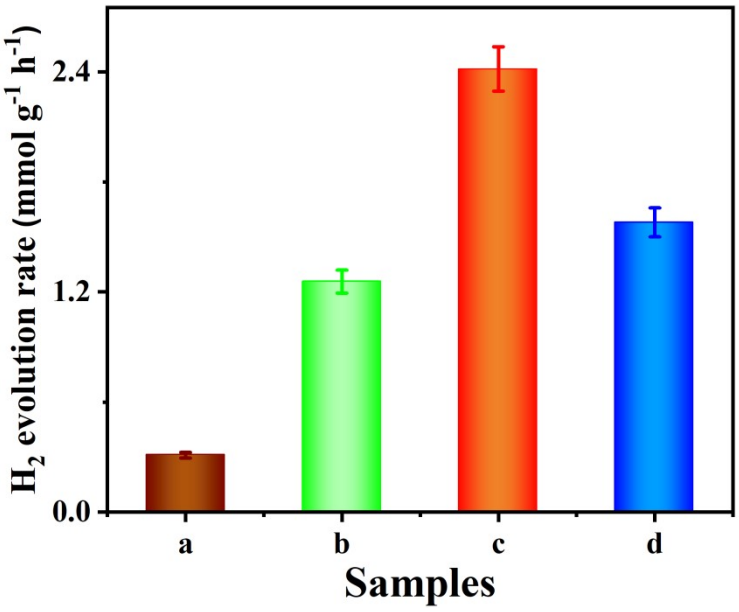

Fig. S1. Photocatalytic H_2-evolution rate of (a) CdS, (b) NiOOH-$Ti_3C_2F_x$(1:5)/CdS-1%, (c) NiOOH-$Ti_3C_2F_x$(1:5)/CdS-5%, and (d) NiOOH-$Ti_3C_2F_x$(1:5)/CdS-10%.

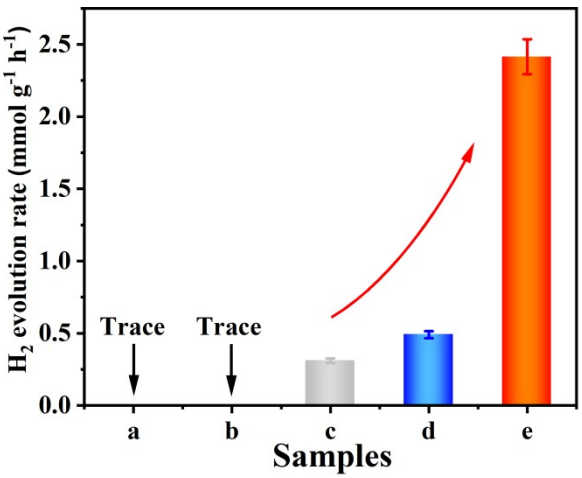

Fig. S2. Photocatalytic H_2-evolution rate of (a) $Ti_3C_2F_x$, (b) NiOOH-$Ti_3C_2F_x$, (c) CdS, (d) $Ti_3C_2F_x$/CdS, and (e) NiOOH-$Ti_3C_2F_x$/CdS.

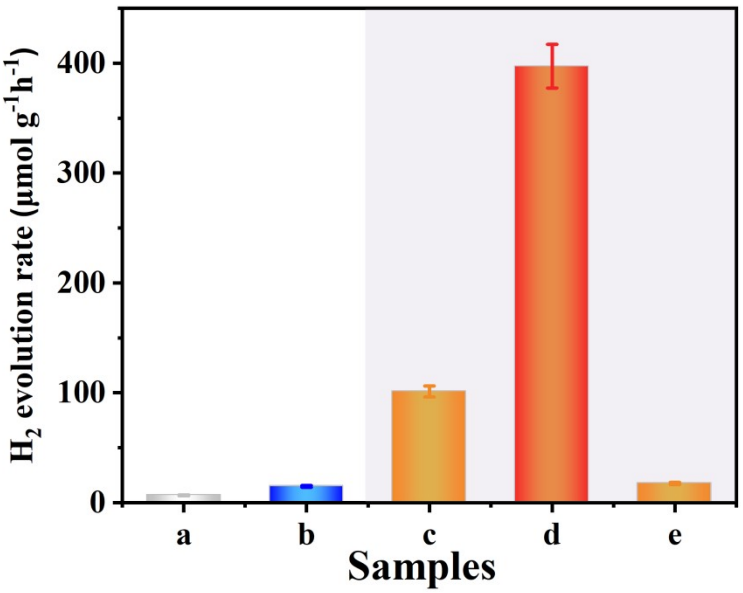

Fig. S3. Photocatalytic H_2-evolution rate of (a) TiO_2, (b) $Ti_3C_2F_x/TiO_2$, (c) NiOOH-$Ti_3C_2F_x$(1:2)/TiO_2, (d) NiOOH-$Ti_3C_2F_x$(1:5)/TiO_2, and (e) NiOOH-$Ti_3C_2F_x$(1:10)/TiO_2.

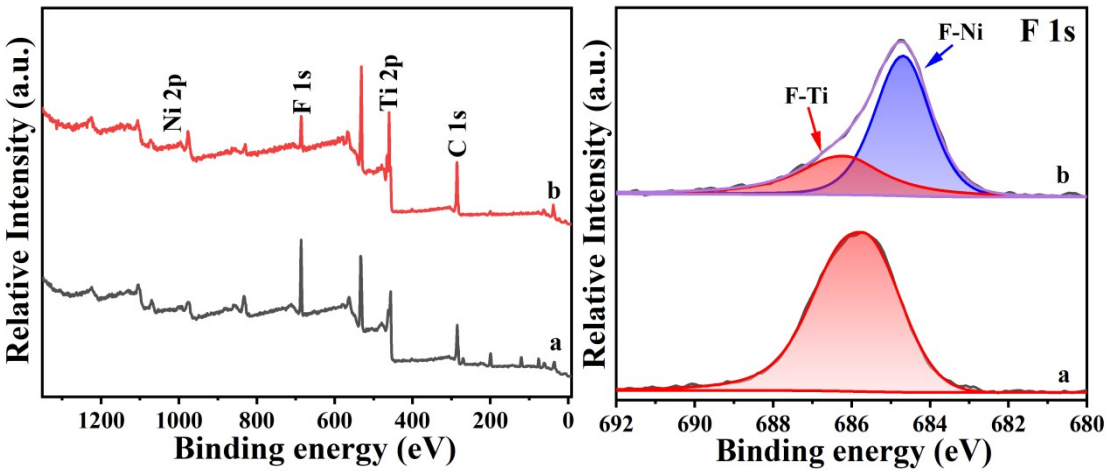

Fig. S4. (A) XPS survey spectra and (B) high-resolution spectra of F 1s for (a) $Ti_3C_2F_x$ and (b) NiOOH-$Ti_3C_2F_x$(1:1).

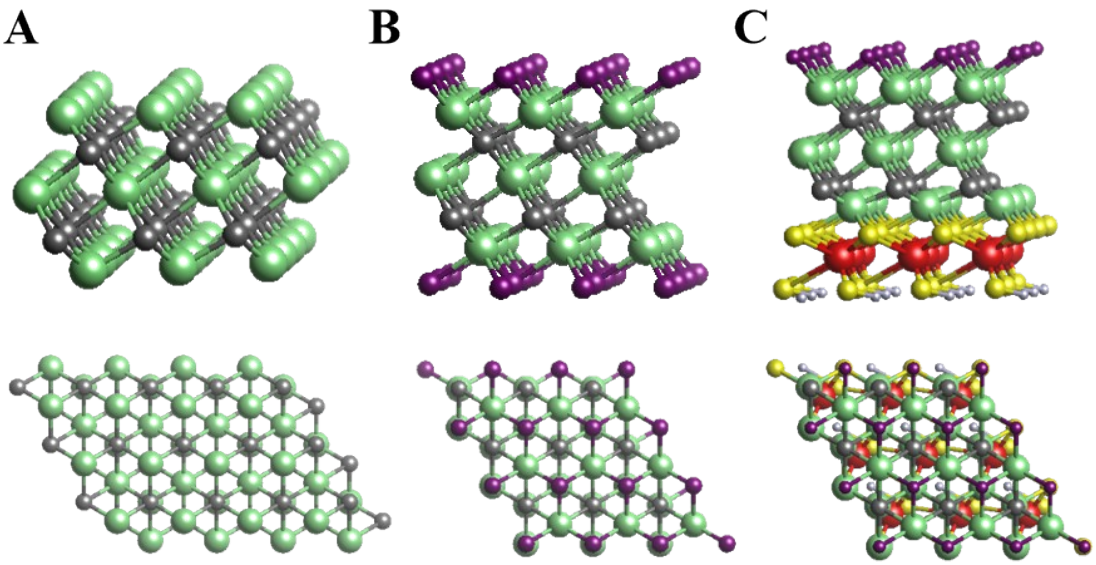

Fig. S5. Front and top views of the optimized models of (A) Ti_3C_2 MXene, (B) $Ti_3C_2F_x$, (C) NiOOH-$Ti_3C_2F_x$.

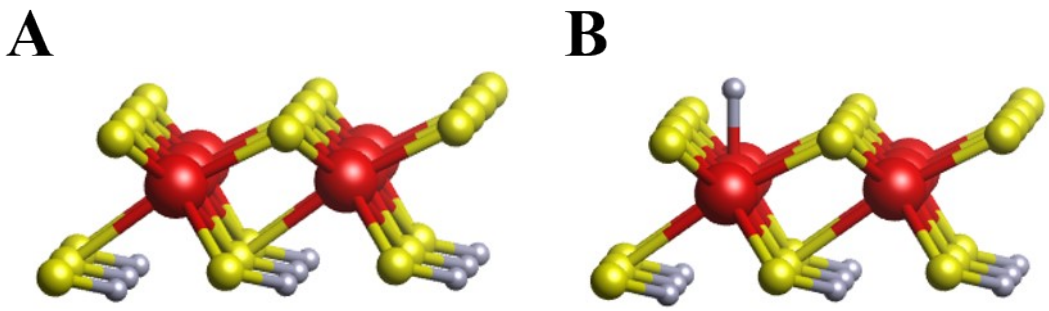

Fig. S6. The optimized models for DFT calculations of (A) NiOOH; (B) H-NiOOH.

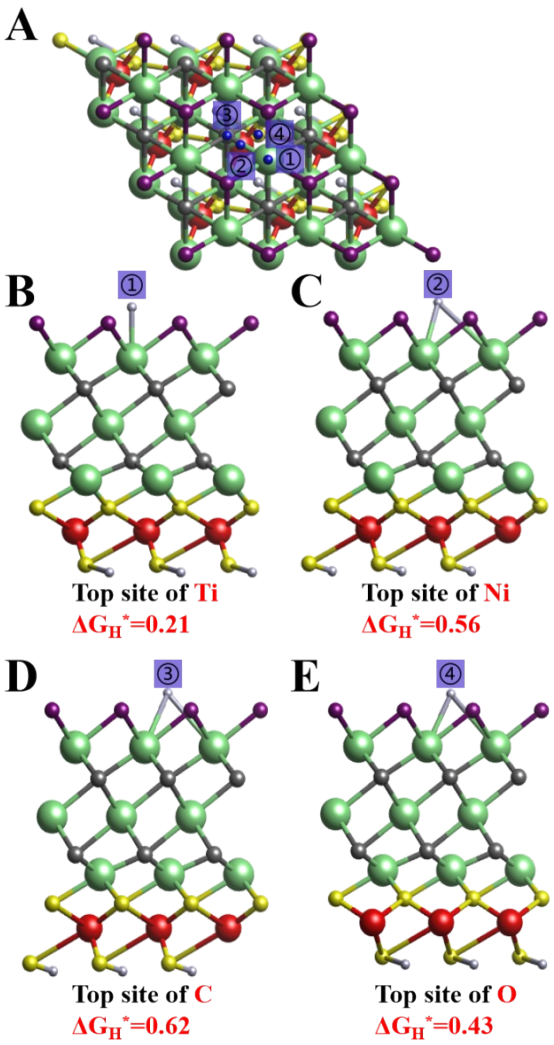

Fig. S7. (A). Top view of the different hydrogen adsorption sites on NiOOH-$Ti_3C_2F_x$; Demonstration of different adsorption sites on NiOOH-$Ti_3C_2F_x$, exemplified by (B). top site of Ti; (C). top site of Ni; (D). top site of C; (E). top site of O.

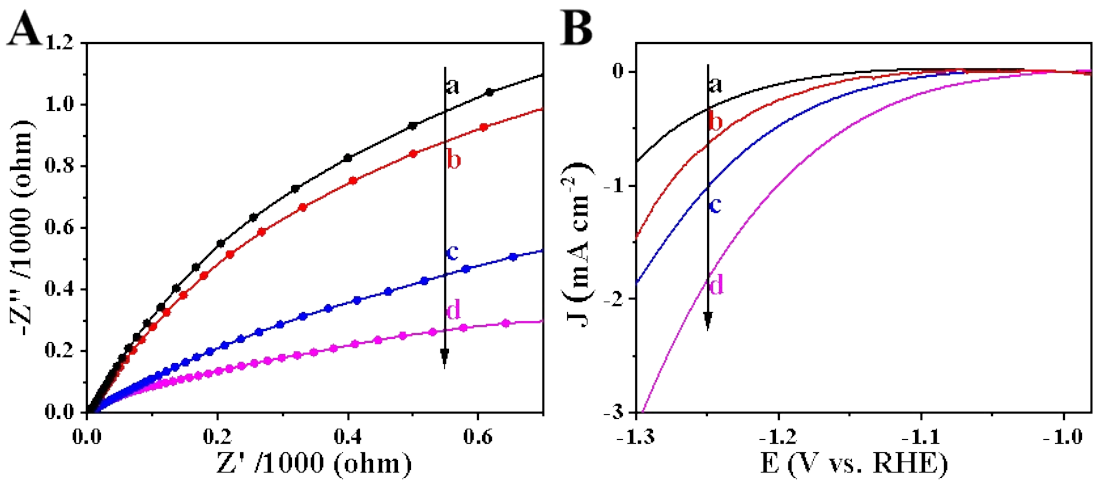

Fig. S8. (A) Electrochemical impedance spectra (EIS) and (B) linear sweep voltammetry (LSV) curves of (a) CdS, (b) $Ti_3C_2F_x$/CdS, (c) NiOOH-$Ti_3C_2F_x$(1:1)/CdS, and (d) NiOOH-$Ti_3C_2F_x$(1:5)/CdS.